

On the Importance of Fiber Curvature to the Elastic Moduli of Electrospun Nonwoven Fiber Meshes

Chia-Ling Pai⁽¹⁾, Mary C. Boyce⁽²⁾, and Gregory C. Rutledge^{(1)*}

⁽¹⁾ Department of Chemical Engineering and ⁽²⁾ Department of Mechanical Engineering, Massachusetts Institute of Technology, 77 Massachusetts Avenue, Cambridge, Massachusetts 02139 USA

*To whom correspondence should be addressed. Tel.: 617-253-0171; fax: 617-258-5776.
E-mail: rutledge@mit.edu

ABSTRACT

Adequate mechanical integrity of nonwoven fabrics is generally a prerequisite for their practical usage. Nonwoven fiber mats of poly(trimethyl hexamethylene terephthalamide) (PA 6(3)T) with average fiber diameters from 0.1 to 3.6 microns were electrospun from solutions in dimethylformamide and formic acid and their in-plane mechanical response characterized. Two quantitative microstructure-based models that relate the Young's moduli of these fabrics to those of the fibers are considered, one assuming straight fibers and the other allowing for curved fibers. It is found that the model allowing for curved fibers provides a quantitative relationship between the Young's moduli of the mats and those of the fibers themselves. The governing factors that affect the mechanical properties of nonwoven mats are the porosity of the mats, the intrinsic fiber modulus, and the average fiber diameter, curvature (or "curl") and distance between fiber-to-fiber junctions. Especially for submicron diameter fibers, both the intrinsic fiber properties and fiber curvature make important contributions to the mechanical behavior of their nonwoven fabrics.

1. Introduction

Polymeric nonwoven fabrics are readily fabricated by the technique called “electrospinning”, which produces an interconnected network of fibers with diameters from a few tens of nanometers to microns, thus resulting in high specific surface area ($\sim 1\text{-}100\text{ m}^2/\text{g}$) and high porosity ($\sim 90\%$) [1]. These fabrics have garnered much attention for their use in applications that benefit from such a high surface area and porous fibrous structure, such as filtration materials, fuel cell membranes, catalytic systems, biological scaffolds and sensors [2-3]. Mechanical integrity is of particular concern for the utility of these mats. Although many experimental and theoretical studies have been conducted on the mechanical properties of traditional nonwoven fabrics, no systematic and comprehensive studies have been reported that can adequately account for the observed mechanical properties of mats comprising relatively small electrospun fibers. For example, fibers have been reported to exhibit enhanced Young’s moduli and yield stresses below a critical diameter, such as 500 nm for poly(trimethyl hexamethylene terephthalamide) (PA 6(3)T) [4], but these enhancements are not reflected in the fiber mats themselves [5].

Models of nonwoven fabrics can be categorized into four main approaches (Jearanisilawong [6]): (i) idealized composite models of homogeneous continuum components that do not consider the structure of the material at the fiber level [7]; (ii) composite structures consisting of many continuum components to represent the idealized elements of the fabric structure [8-10]; (iii) complex fiber network structures that capture the macroscopic response of the fabric from the interactions between the components of the structure at the fiber and bond level [11]; and (iv) both continuum- and microstructurally-based approaches that use a representative volume element of the material to homogenize the macroscopic response of nonwoven fabrics [12,13]. Our goal in this work is to understand how the fiber properties and mat microstructure translate to the elastic mechanical properties of the mat, for which purpose the microstructurally-based continuum approach is most appropriate to model the mat.

Of particular importance in determining the elastic response of nonwoven mats is the role of fiber curvature and bending. The importance of this feature was recognized already in the seminal work of Backer and Petterson [7]. Hearle and co-workers [8,9]

were the first to account for this fiber "curl" in a microstructural model, using the approximation that only fully straightened fibers contribute to the elastic properties of a mat. Lee and Argon [10] studied the flexibility of crimped fibers in sinusoidal shape subjected to tension. Adanur and Liao [14] adopted the same approximation as Hearle and Newton for fiber curl. More recently, Engelmayr and Sacks [15] were the first to include finite contributions to elastic modulus due to fiber bending in their study of needle-punched nonwoven tissue engineering scaffolds. In that work, the fibers were imparted with an intrinsic, sinusoidal curvature by crimping, as part of the nonwoven fabrication process, and the materials were then evaluated in flexure. In this paper we present a relatively simple model that can relate the Young's modulus of single fibers to their nonwoven fabrics, and vice versa, focusing on electrospun polymeric fibers for experimental validation.

2. Experimental Section

2.1. Materials. Poly(trimethyl hexamethylene terephthalamide) (PA 6(3)T, $M_v = 15$ kg/mol, $\rho = 1.12$ g/cm³, $T_g = 140^\circ\text{C}$) was purchased from Scientific Polymer Product, Inc. Dimethylformamide (DMF) (ACS reagent, >99.8%) and formic acid (FA) (ACS reagent, 96%) were purchased from Sigma Aldrich, Inc. All materials were used without further purification.

2.2. Sample Preparation. PA 6(3)T was dissolved in DMF to form 30 wt% and 36 wt% solutions, and in a mixture of DMF/FA with the weight ratio of 99:1 to form 22 wt%, 28 wt%, and 30 wt% solutions. All solutions were prepared at room temperature. Fiber mats were fabricated by electrospinning using an apparatus similar to that reported by Shin et al [16], where a parallel-plate configuration was used to obtain a uniform applied electric field and to eliminate corona discharges. The plate-to-plate distance (D) was varied from 33 to 53.5 cm. The flow rate (Q) and voltage (V) were varied from 0.002 to 0.05 ml/min and from 30 to 40 kV, respectively. Detailed electrospinning conditions can be found in Table 1 of ref [4]. Randomly distributed nonwoven meshes were collected on a grounded aluminum foil for later characterization.

2.3. Characterization. Scanning electron microscopy (SEM) (JEOL-6060SEM, JEOL Ltd., Japan) was used at 5 to 10 kV acceleration voltage and 15 mm working

distance for morphological characterization and determination of fiber diameter. PA 6(3)T does not exhibit any significant crystallinity. The absence of both beads and pores was confirmed by SEM, as reported previously [4]. The random orientation of fibers within the plane of the mats was confirmed by image analysis of SEM micrographs, as described in the Appendix. A Zwick mechanical tester, model BTC-EXMACRO.001 (Roell, Germany), was used to measure the Young's moduli of nonwoven meshes in uniaxial tension at a constant strain rate of 10^{-3} s^{-1} , which is equal to a crosshead speed of 1.8 mm/min for a sample length of 7 cm, and gauge length between grips of 3 cm. The sample width was 0.7 cm, which gives a gauge length to width ratio greater than 3; our related work [17] found that a grip-to-grip gauge length/width ratio of 3 provides for uniaxial tension conditions of these specimens, while ratios less than 2.5 are constrained and the grip effect interferes with contraction. An Autopore IV 9500 mercury penetrometer (Micromeritics, Norcross, GA) was used to measure the porosity of nonwoven fabrics. An adjustable Measuring Force Digimatic Micrometer (Model CLM1 .6"QM, Mitutoyo, Japan) was used to measure the thickness of nonwoven fabrics at 0.5 N (or 0.0177 MPa), the minimum measuring force allowed by this micrometer. Using a normal micrometer to measure thickness of a nonwoven electrospun fabric was generally found to over-compress the sample and underestimate its thickness, and thus overestimate the Young's modulus.

3. Theoretical Section

3.1. Nonwoven Fabric Model for Straight Fibers. The constitutive model for a two-dimensional network of fibers of nonwoven mats is developed here using a 4-fiber construction as the representative volume element (RVE) [12,13], as shown in Fig. 1. The model is two-dimensional and the initial fiber orientation angle, θ_0 , is uniformly distributed between 0 and 180 degrees for an isotropic planar network. Individual fibers are allowed to rotate and to extend or compress. A torsional resistance captures the junction stiffness and the effective influence of laterally oriented fibers, which also restrict rotation of other fibers; it is shown schematically in Fig. 1 by a rotational Hookean spring.

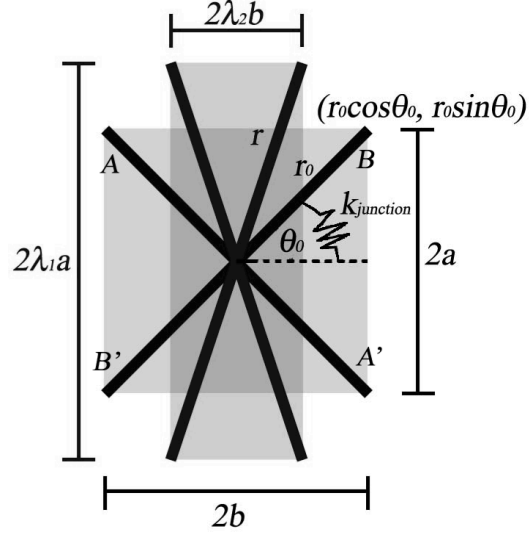


Figure 1. Schematic of a 4-fiber model with square region ($2a \times 2b$) representing the RVE before deformation and the rectangular region ($2\lambda_1 a \times 2\lambda_2 b$) representing the RVE after deformation.

A strain energy density function is constructed for this 4-fiber micromechanical model by mapping the macroscopic mat deformation to the microscopic fiber deformation and then determining expressions for the contributions to strain energy from the deformation of the fibers and the junctions. The model includes finite contributions to the energy of deformation from stretching of straight fibers, bending or unbending of curved fibers and torsional resistance at junction points.

The fiber extension and the junction rotation are determined in terms of the macroscopic deformation, which are then used together with fiber force-extension and junction torsion-rotation relations to obtain strain energy. The macroscopic deformation gradient is:

$$F_{2D} = \frac{\partial x}{\partial X} = \begin{bmatrix} F_{11} & F_{12} \\ F_{21} & F_{22} \end{bmatrix} = \begin{bmatrix} \lambda_1 & 0 \\ 0 & \lambda_2 \end{bmatrix} \quad (1)$$

where x is the deformed position of a material point, X is the reference position, and λ_i is one of the two principal stretches within the plane.

The stretch ratio of the constituent fibers in the four-fiber network RVE is kinematically determined:

$$\lambda_f = \frac{r}{r_0} = \left(\lambda_1^2 \sin^2 \theta_0 + \lambda_2^2 \cos^2 \theta_0 \right)^{1/2} \quad (2)$$

where r_0 is the initial fiber length between junctions, r is the deformed fiber length, and $\theta_0 = \tan^{-1}(a/b)$ is the angle between the initial fiber orientation and the lateral axis.

The fiber strain energy is:

$$u_f = \frac{1}{2} k_f r_0^2 (\lambda_f - 1)^2 \quad (3)$$

where $k_f = E_f A_f / r_0$ is the fiber axial stiffness for a Hookean spring, in units of force per unit length, with E_f being the fiber modulus and A_f being the fiber cross-sectional area.

The strain energy contribution from the junction is given by [18]:

$$u_{junction} = \frac{1}{2} k_{junction} (\theta - \theta_0)^2 \quad (4)$$

where $k_{junction}$, the effective torsional stiffness with the unit of J/rad², captures the effective torsional stiffness from the junction as well as the effect of lateral fibers in restricting junction rotation.

The strain energy density for the RVE containing 4 fibers (A, A', B, and B') is then given by:

$$u^* = \frac{\nu}{n} \left[\left(\sum_{i=1}^{n=4} u_i \right) + u_{junction} \right] = \frac{\nu}{2} k_f r_0^2 (\lambda_f - 1)^2 + u_{junction}^* = \nu u_f + u_{junction}^* \quad (5)$$

where ν is the areal density (number of fibers per unit area), and $u_{junction}^* = \nu u_{junction} / n$.

The Cauchy stress tensors can be calculated from the following equations:

$$T_1 = \frac{1}{J} \frac{\partial(vu_f)}{\partial F_{11}} F_{11}^T + \frac{\lambda_1}{J} n_{junction} k_{junction} (\theta - \theta_0) \frac{\partial \theta}{\partial \lambda_1}; \quad (6a)$$

$$T_2 = \frac{1}{J} \frac{\partial(vu_f)}{\partial F_{22}} F_{22}^T + \frac{\lambda_2}{J} n_{junction} k_{junction} (\theta - \theta_0) \frac{\partial \theta}{\partial \lambda_2} = 0 \quad (6b)$$

where $J = \det(F) = \lambda_1 \lambda_2$ is the ratio of planar deformed area to original area, and $n_{junction}$ is the number density of junctions per unit area within the network. For the uniaxial tension experiments described in this work, deformation in the lateral direction is unrestricted, so that T_2 is identically equal to zero. The condition $T_2 = 0$ together with a measure of the lateral stretch, λ_2 , during uniaxial tension provides the equation needed to determine $k_{junction}$. Our measurements indicate that λ_2 is approximately unity at small elastic strains for these electrospun mats.

The derivatives of the chain angle with respect to the principal stretches can be expressed as:

$$\frac{\partial \theta}{\partial \lambda_1} = \frac{\partial \cos^{-1}\left(\lambda_2 / \sqrt{\lambda_1^2 + \lambda_2^2}\right)}{\partial \lambda_1} = \frac{\lambda_2}{\left(\lambda_1^2 + \lambda_2^2\right)}; \quad (7a)$$

$$\frac{\partial \theta}{\partial \lambda_2} = \frac{\partial \cos^{-1}\left(\lambda_2 / \sqrt{\lambda_1^2 + \lambda_2^2}\right)}{\partial \lambda_2} = \frac{-\lambda_1}{\left(\lambda_1^2 + \lambda_2^2\right)} \quad (7b)$$

Using Eq. (6b), we can substitute $n_{junction} k_{junction}$ in Eq. (6a) with a function containing the principal stretches and the angle.

Young's modulus of the nonwoven fabric can be derived from the first derivative of the Cauchy stress in Eq. (6a) with respect to the principal stretch in the direction of uniaxial deformation, averaged over the distribution of initial fiber orientations:

$$E_{mat} = \frac{1}{t_{mat}} \left\langle \frac{\lambda_1 \partial T_1}{\partial \lambda_1} \Big|_{\lambda_1=1} \right\rangle = \frac{\nu k_f r_0^2 \langle \sin^2 \theta_0 \rangle}{t_{mat}} \quad (8)$$

where t_{mat} represents the thickness of the nonwoven mat.

For a nonwoven mesh of randomly oriented fibers, the two-dimensional ensemble average is $\langle \sin^2 \theta_0 \rangle = \int_0^\pi \sin^2 \theta_0 d\theta_0 / \int_0^\pi d\theta_0 = 1/2$, so that:

$$E_{mat} = \frac{\nu k_f r_0^2}{2t_{mat}} \quad (9)$$

The relation between k_f and the Young's modulus of single fibers, E_f , is:

$$k_f = \frac{E_f A_f}{r_0} = \frac{E_f (\pi d^2 / 4)}{r_0} \quad (10)$$

where A_f is the cross sectional area of a fiber, and d is the fiber diameter. Combining Eq. (9) and Eq. (10) yields a result that is equivalent to Cox's model in two dimensions [19].

The volume of solid fibers constituting the nonwoven fabric, V_f , is equal to the product of the total number of fibers in the nonwoven mat (N) multiplied by the volume of each fiber ($A_f r_0$). The volume of the nonwoven fabric, V_{mat} , is equal to the product of the width, length, and thickness of the nonwoven mat ($W_{mat} \cdot L_{mat} \cdot t_{mat}$).

The porosity, ϕ , of the nonwoven mat can be expressed in terms of either the basis weight, $b.w. = m/W_{mat}L_{mat}$, or the areal density, ν , of the mat:

$$1 - \phi = \frac{V_f}{V_{mat}} = \frac{m / \rho_f}{W_{mat} L_{mat} t_{mat}} = \frac{(b.w.) / \rho_f}{t_{mat}} = \frac{N A_f r_0}{W_{mat} L_{mat} t_{mat}} = \frac{\nu A_f r_0}{t_{mat}} \quad (11)$$

where m is the sample mass and ρ_f is the material density of the fibers. We rearrange Eq. (11) to obtain an expression for ν :

$$\nu = \frac{(b.w.)}{\rho_f r_0 A_f} \quad (11')$$

We substitute Eq. (10) and Eq. (11') into Eq. (9) to replace parameters k_f and ν by parameters that can be measured easily:

$$E_f = \frac{2\rho_f}{(b.w.)} E_{mat} t_{mat} = \frac{2\rho_f}{(b.w.)} \frac{\Delta F}{W_{mat} \Delta \epsilon} \Big|_{elastic} \quad (12)$$

We measure the width, length, and mass of the nonwoven sample with known material density of the fibers. From the elastic region of mechanical testing, the Young's modulus of fibers can be estimated by the second equality in Eq. (12), which avoids the problematic determination of t_{mat} . This problem arises because, for soft materials like electrospun mats, the thickness measured by a micrometer is sensitive to the pressure at which the measurement is made. It is desirable therefore to avoid characterizing the material in terms of properties that depend on mat thickness. Determination of E_{mat} , however, does depend on t_{mat} . For this reason, thicknesses should be reported using a consistent measurement pressure, or else extrapolated to zero pressure from measurements at several pressures.

3.2. Nonwoven Fabric Model for Curved Fibers. Up to this point, all fibers have been assumed to be straight, responding to an imposed deformation by changing length and rotating in response to the applied force. However, electrospun fibers generally are observed by SEM to have some degree of curvature [15]. Such fibers can respond to deformation by bending or unbending. Hearle and coworkers [8,9] defined the ‘‘curl’’ factor, c , as the ratio of the actual curved fiber length to the straight length between the ends of the element. However, they then took the energy of fiber deformation to be zero for fibers with $c > 1$. Here, we explicitly include the finite bending energy, which plays a

prominent role in governing the modulus of the electrospun mats, particularly those of submicron diameters. A modified version of the foregoing model that includes consideration of the initial curvature of the fiber and the bending or unbending on the change of fiber stiffness is shown in Fig. 2.

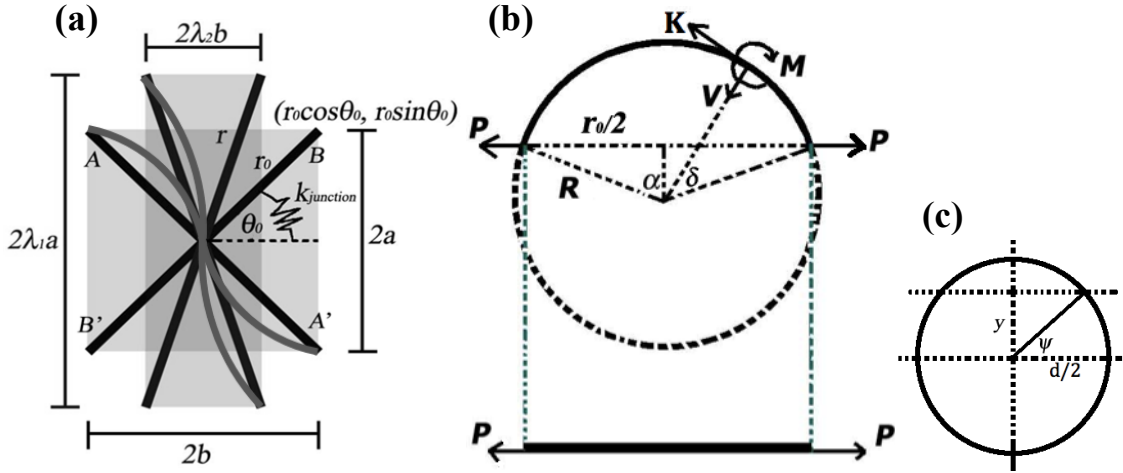


Figure 2. (a) Schematic of curved fibers in the RVE; (b) schematic of a fiber with a radius of curvature R , and a straight fiber with zero curvature (infinite radius of curvature) and fiber length r_0 , under the same loading force P ; (c) cross-section of a fiber with diameter d , and arbitrary $y = \sin \psi \cdot d/2$.

First, the force and moment balances for the curved fiber segment are expressed by the following equations:

$$\text{Force balance: } K \cos(\alpha - \delta) + V \sin(\alpha - \delta) = P \quad (13a)$$

$$K \sin(\alpha - \delta) = V \cos(\alpha - \delta) \quad (13b)$$

$$\text{Moment balance: } M = P \left(R \cos(\alpha - \delta) - \sqrt{R^2 - (r_0 / 2)^2} \right) \quad (14)$$

where P is the applied load, which resolves into K and V , the axial and transverse forces acting at any point on the fiber, $\alpha = \arcsin(r_0/2R)$, and ψ is an arbitrary angle. M is the

moment, R is the radius of curvature, and r_0 is the distance between two junction points along a fiber.

From Eq. (13a) and (13b), we find:

$$K = P \cos(\alpha - \delta) \quad (15)$$

We also need to formulate the axial stress distribution across any cross-section of the fiber in order to calculate the strain energy.

$$\text{Axial stress: } \sigma_{axial} = -\frac{My}{I} + \frac{K}{A_f} \quad (16)$$

where M varies along the fiber as described by Eq. (14), y is shown in Fig. 2(c), and $I = \pi d^4 / 64$. Note in particular that the second moment of area, I , is proportional to the fourth power of fiber diameter, which accounts for the tendency of smaller fibers to have smaller resistance to bending.

The strain energy is:

$$U = \int_{V_f} \frac{\sigma_{axial}^2}{2E_f} dV = \frac{1}{2E_f} \int_{V_f} \left(\frac{M^2 y^2}{I^2} - \frac{2MyK}{IA_f} + \frac{K^2}{A_f^2} \right) dV \quad (17)$$

where $dV = dA(Rd\delta)$. After the integration, $U = P^2\beta$, where:

$$\beta = \left[\frac{R^3}{2E_f I} \alpha + \frac{R^3}{4E_f I} \sin(2\alpha) - \frac{2R^2 \sqrt{R^2 - (r_0/2)^2}}{E_f I} \sin \alpha + \frac{(R^2 - (r_0/2)^2)R}{E_f I} \alpha + \frac{R\alpha}{2E_f A_f} + \frac{R \sin(2\alpha)}{4E_f A_f} \right] \quad (18)$$

The displacement can be calculated by $\delta = \frac{\partial U}{\partial P} = 2P\beta$.

As a result $U = \delta^2 / 4\beta = k_{cf} \delta^2 / 2$, where the apparent stiffness of curved fibers, $k_{cf} = 1 / (2\beta)$.

We define the stiffness ratio (SR) as the ratio of the stiffness of a curved fiber to the stiffness of a straight fiber of same end-to-end length, which can be expressed as follows:

$$SR = \frac{E_{cf}}{E_f} = \frac{2k_{cf} (r_0 / 2) / A_f}{2k_f (r_0 / 2) / A_f} = \frac{1 / (2\beta)}{k_f} \text{ with } 0 < SR \leq 1 \quad (19)$$

SR can be rewritten as a function of only junction length (r_0), fiber diameter (d), and radius of curvature (R):

$$\frac{1}{SR} = \left[\frac{8R^3}{d^2 (r_0 / 2)} \operatorname{asin} \left(\frac{r_0 / 2}{R} \right) - \frac{24R \sqrt{R^2 - (r_0 / 2)^2}}{d^2} + \frac{16 (R^2 - (r_0 / 2)^2) R}{d^2 (r_0 / 2)} \operatorname{asin} \left(\frac{r_0 / 2}{R} \right) + \frac{R}{2 (r_0 / 2)} \operatorname{asin} \left(\frac{r_0 / 2}{R} \right) + \frac{\sqrt{R^2 - (r_0 / 2)^2}}{2R} \right] \quad (20)$$

For mats comprising curved fibers, E_f in Eq. (12) can simply be replaced by E_{cf} . As a limiting case, $R \rightarrow \infty$, $\sin \alpha \rightarrow \alpha = (r_0 / 2) / R$, and $R \gg r_0 / 2$, which leads to $SR = 1$, in agreement with the case for straight fibers.

4. Results and Discussion

PA 6(3)T was electrospun to form nonwoven fabrics consisting of homogeneous and smooth fibers over a wide range of fiber diameters, from 113 nm to 3643 nm, as shown in Fig. 3. Results are listed in Table 1 for tensile deformation of nonwoven fabrics with randomly oriented fibers of different average fiber diameter. At least four nonwoven fabrics were tested for each average fiber diameter. The basis weight, width of the sample (0.7 cm), and force vs strain were measured. The material density of PA 6(3)T is known to be 1.12 g/cm³ [20].

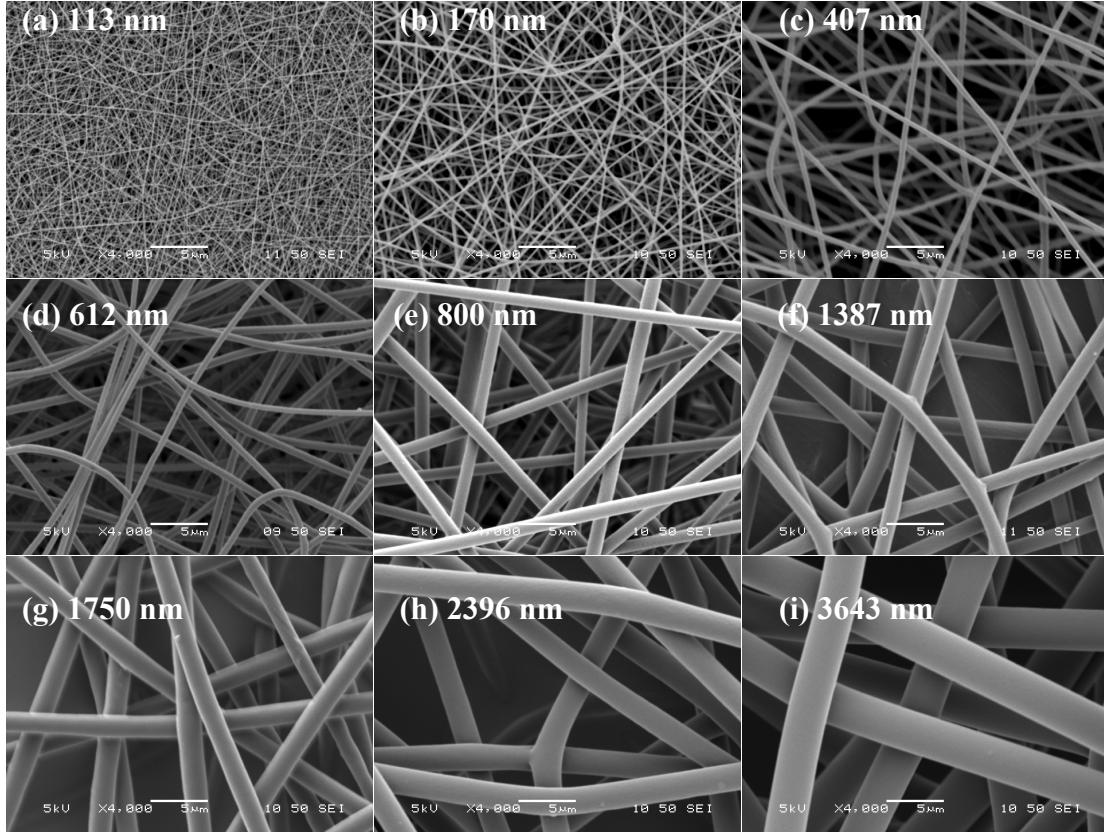


Figure 3. Representative SEM images of PA 6(3)T nonwoven fabrics with different diameters (scale bar = 5 μm).

Table 1: Data for nonwoven fabrics with different average fiber diameters.

d (μm)	$b.w.$ (g/m^2)	$\Delta F/\Delta\varepsilon _{\text{elastic}}$ (N)	R (μm)	ϕ
0.113 ± 0.030	3.1 ± 0.4	10.4 ± 2.2	-	$0.925\pm 0.001^*$
0.128 ± 0.023	3.1 ± 0.4	9.3 ± 1.3	-	-
0.143 ± 0.035	1.9 ± 0.2	6.1 ± 1.8	20 ± 30	-
0.170 ± 0.026	5.1 ± 0.3	17.6 ± 0.6	-	-
0.288 ± 0.027	9.0 ± 0.6	26.5 ± 3.9	44 ± 72	0.914 ± 0.007
0.385 ± 0.039	9.7 ± 0.8	30.4 ± 6.0	-	0.906 ± 0.003
0.407 ± 0.055	13.9 ± 0.6	47.0 ± 11.1	64 ± 97	0.905 ± 0.003
0.612 ± 0.054	22.0 ± 0.9	62.8 ± 8.0	-	0.906 ± 0.006
0.800 ± 0.100	11.0 ± 0.5	36.1 ± 2.5	-	0.888 ± 0.010
1.040 ± 0.161	9.1 ± 0.7	28.0 ± 1.6	181 ± 402	$0.915\pm 0.002^*$
1.290 ± 0.157	5.2 ± 0.7	21.1 ± 2.7	-	$0.904\pm 0.003^*$
1.387 ± 0.128	11.3 ± 0.2	45.4 ± 9.2	-	0.892 ± 0.002
1.750 ± 0.185	12.7 ± 3.1	44.4 ± 6.6	-	-
1.840 ± 0.253	13.6 ± 1.2	44.3 ± 6.2	340 ± 730	0.888 ± 0.010

2.240±0.178	12.6±0.1	38.2±9.9	-	-
2.396±0.093	14.5±0.3	57.2±7.3	-	0.899±0.002
3.643±0.070	39.9±2.4	185.0±25.0	-	0.875±0.005

The values indicated by \pm correspond to one standard deviation. The values of porosity indicated by a “*” were measured by mercury porosimetry; the rest of porosities were measured gravimetrically, using the micrometer with 0.5 N force to determine t_{mat} . The “-” indicate values that were not determined in this work.

The thickness of the nonwoven fabrics, t_{mat} , can be measured by the micrometer with a constant pressure (0.0177 MPa), or calculated using Eq. (11) with the porosity, ϕ , measured by mercury porosimetry, for example. Thus, we can choose to measure either porosity and calculate thickness, or vice versa. Using the micrometer and Eq. (11), the porosity for the nonwoven fabrics with average fiber diameter from 113 nm to 3643 nm varies from about 0.875 to 0.914; using mercury porosimetry, it varies from about 0.904 to 0.925, as shown in Table 1. This range of variation is considered to be very slight, with only a modest tendency towards higher porosity values for mats of smaller fibers. Pham et al. [21] also observed a relatively consistent porosity for poly(ϵ -caprolactone) microfiber scaffolds with average fiber diameters ranging from 2 to 10 μm . The somewhat larger discrepancy between techniques can be attributed to both the small sample sizes analyzed by mercury porosimetry, which necessitates mass determinations accurate to four significant digits, and the finite compression of the samples under the micrometer, which tends to systematic underestimation of thickness, and thus also porosity. As an aside, it is worth noting that the high pressures employed by mercury porosimetry also lead to deformation of the sample, giving rise to possible errors in the determination of pore size distributions, as described elsewhere [22]. In light of these uncertainties, in the analysis to follow, where necessary, we used porosities ranging from 0.90 (for the smallest fibers) to 0.88 (for the largest fibers), as shown in Table 2.

Representative stress-strain curves for nonwoven mats comprising different fiber diameters are shown in Fig 4(a). The mats with smaller fiber diameter exhibit lower yield stresses and less elongation to break than those with larger fiber diameter. All of the samples show a maximum in stress, followed by a gradual failure indicative of rupture of the fibers and inter-fiber junctions. The dependence of the Young’s modulus of

nonwoven fabrics on fiber diameter is plotted in Fig. 4(b); the error bars corresponds to one standard deviation, due to the variation between samples. E_{mat} is observed to decrease slightly with decreasing fiber diameter.

Using Eq. (12), derived for the model of straight fibers, the fiber modulus E_f can be calculated; the resulting values are listed in the second column of Table 2. We plot these values of E_f in Fig. 5, shown as the filled diamond symbols, and compare with data obtained from direct measurements of individual fibers, shown as the open triangular symbols. Individual fiber measurements were performed by tensiometry using a U9815A UTM T150 universal testing system (Agilent Technologies, Santa Clara, CA) and have been reported previously [4]. We found that the Young’s moduli of fibers derived from the measurement of nonwoven fabrics assuming straight fibers all fall below the values measured directly for single fibers, and tend towards lower values with decreasing fiber diameter, in contrast to the single fiber data. These discrepancies suggest that the simple model based on straight fibers does not suffice to describe the relation between fiber modulus and mat modulus for these nonwoven fabrics.

Table 2: Fiber moduli derived from mat properties and microstructural models. “model 1” refers to straight fibers; “model 2” refers to curved fibers.

d (μm)	E_f (model 1) (GPa)	ϕ	R (μm)	r_o (μm)	SR	E_f (model 2) (GPa)
0.113±0.030	1.05	0.90	15	3.3	0.15	6.83
0.128±0.023	0.98	0.90	18	4.0	0.16	6.21
0.143±0.035	1.01	0.90	20	4.2	0.16	6.25
0.170±0.026	1.12	0.90	24	5.0	0.17	6.69
0.288±0.027	0.95	0.90	43	8.4	0.19	5.03
0.385±0.039	1.00	0.90	60	11.2	0.20	4.93
0.407±0.055	1.08	0.90	64	11.8	0.21	5.25
0.612±0.054	0.92	0.90	100	17.5	0.23	4.01
0.800±0.100	1.06	0.89	135	22.7	0.25	4.27
1.040±0.161	0.99	0.89	181	29.1	0.27	3.66
1.290±0.157	1.32	0.89	229	35.5	0.29	4.53
1.387±0.128	1.28	0.89	249	38.0	0.30	4.27
1.750±0.185	1.11	0.89	322	46.9	0.33	3.38
1.840±0.253	1.04	0.89	340	49.1	0.34	3.10
2.240±0.178	0.96	0.89	423	58.4	0.37	2.62

2.396±0.093	1.26	0.89	456	62.0	0.38	3.34
3.643±0.070	1.49	0.88	726	88.1	0.46	3.20

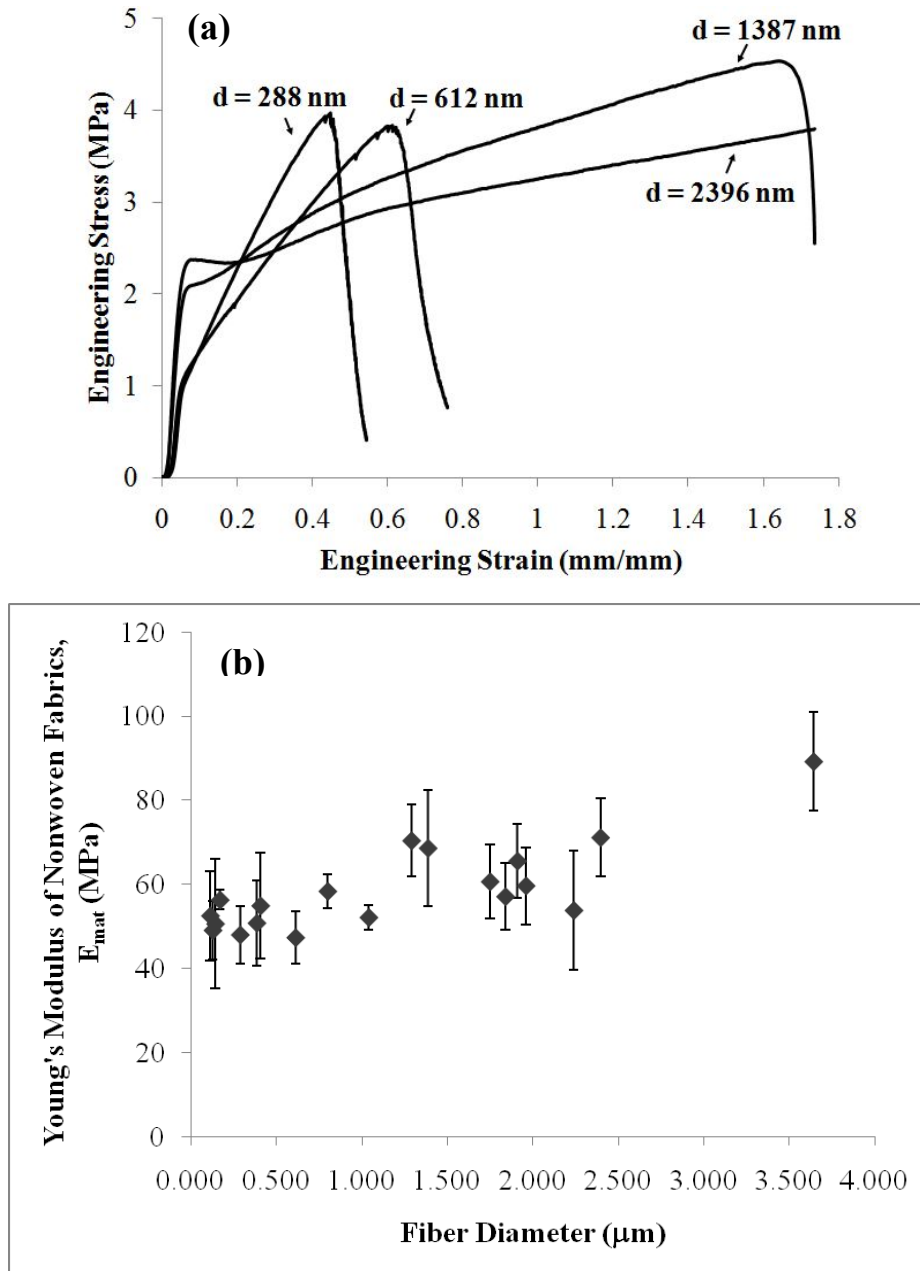


Figure 4. (a) Representative stress-strain curves of nonwoven fabrics. (b) Dependence of Young's modulus of nonwoven fabrics on fiber diameter.

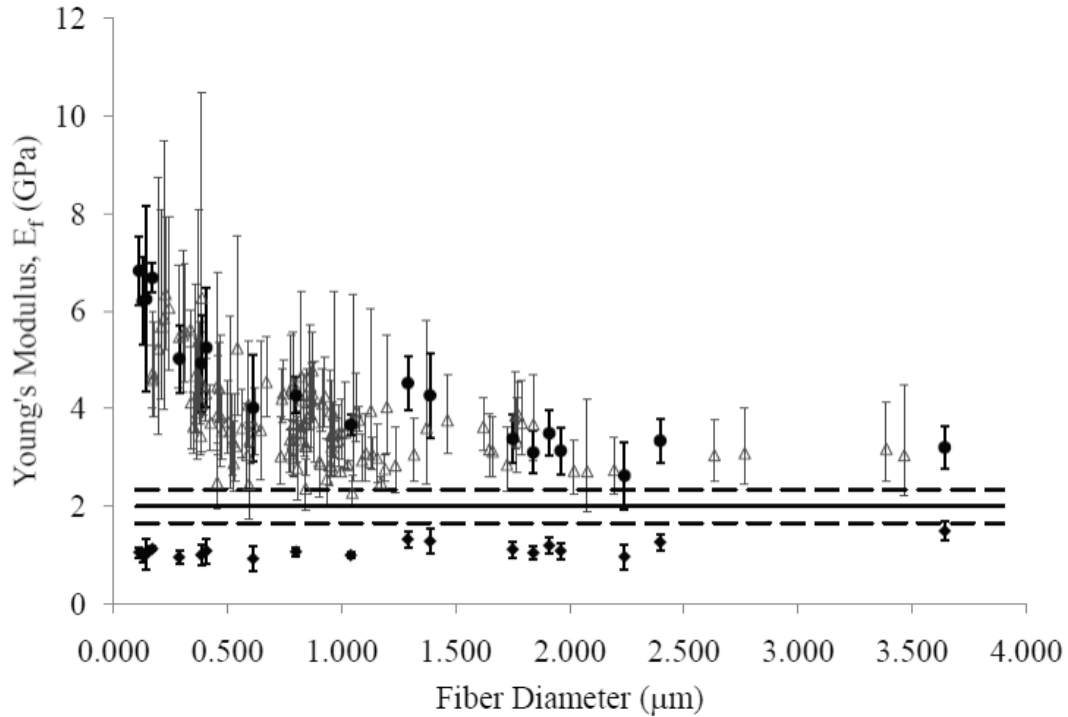


Figure 5. Dependence of Young's modulus of single fibers on fiber diameter. Open triangles represent experimental data in uniaxial extension [4]; filled diamonds represent derived Young's moduli of the single fibers from mat data assuming straight fibers, and filled circles represent those assuming curved fibers. Solid lines represent experimental values for bulk films, and dashed lines represent one standard deviation.

It is apparent from Fig. 3 and similar images of nanofiber nonwoven fabrics that the fibers are distinctly curved, especially for the smallest diameter fibers. Therefore, the original four-fiber model was modified by replacing straight fiber elements with curved fiber elements, as described in the Theoretical Section. As shown by Eq. (19) and Eq. (20), the Young's modulus of curved fibers is equal to the apparent modulus predicted by Eq. (12) divided by the stiffness ratio, SR . In order to evaluate SR , two additional characteristics of the nonwoven mat are required: the through-space distance between consecutive junctions along a fiber (r_0) and the radius of curvature (R). For purposes of this work, these characteristics were measured manually from SEM images as illustrated in Fig. 6 and described below; however, automation of this procedure can be readily envisioned.

The radius of curvature is determined by first tracing visually along a fiber and identifying the coordinates of points where the fiber appears to cross, or form a junction with, another fiber. Second, three consecutive points (identified as “1”, “2” and “3” in Fig 6) are used to construct a circle, from which the radius of curvature is obtained. The average radius of curvature was calculated for five samples of different average fiber diameter spanning about one order of magnitude, using about 300 circles per sample. For our PA 6(3)T mats, the results can be described empirically by a power law of the form $R = Ad^n$. From the plot shown in Fig 7(a), A and n were found to be 173 ± 17 and 1.1 ± 0.1 , respectively, and hence the radius of curvature was found to be nearly linearly dependent on the fiber diameter. This linear relationship makes sense because the radius of curvature should be equal to $E_f I / M$. I is proportional to d^4 while M , a product of a force on impact with the plate (which scales with $\sim d^2$) and the moment arm (which scales with $\sim d$), is proportional to d^3 , so that R scales linearly with d . This relation was then used to estimate the radius of curvature for all of the mats; experimental data are listed in Table 1 and values estimated from Fig 7a are listed in Table 2.

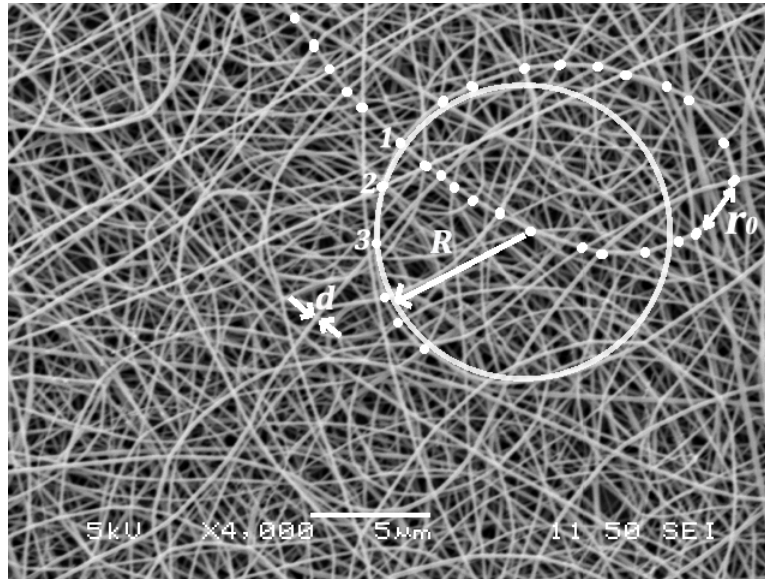


Figure 6. Schematic illustration of the determination of radius of curvature (R), the distance between the junctions along a fiber (r_0), and the average diameter of fibers (d), from image analysis of SEM micrographs.

(a)

(b)

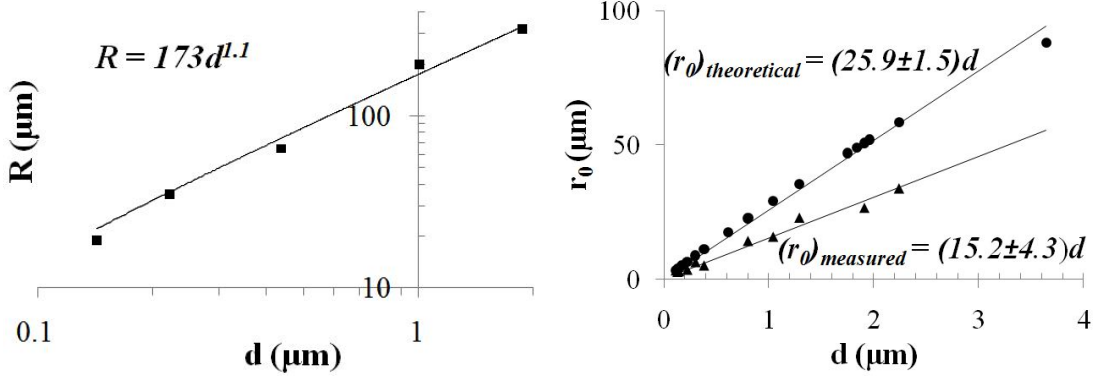


Figure 7. Empirical correlations for radius of curvature (R) and junction distance (r_0) as functions of average diameter of fibers in mats. (a) Radius of the curvature; (b) measured distance (filled triangles) and theoretical distance (filled circles) between junctions.

The identification of points where fibers cross (“junctions”) in an SEM image is rather subjective, due to the depth of field that leads to imaging of several layers simultaneously, depending on fiber diameter. Not all such crossings are true junctions. While the determination of radius of curvature is not very sensitive to over- or under-reporting of junctions, the determination of the distance between adjacent junctions (r_0) is very sensitive to such errors. Using the naked eye to distinguish junction points in SEM images yielded the results shown in Fig. 7(b). For comparison, a theoretical relation for the mean pore radius in a nonwoven fiber mat derived by Sampson [23] was also used to approximate the distance between the junctions along a fiber, r_0 :

$$r_0 = -\frac{d\sqrt{\pi}}{2} \left(1 + \frac{\pi}{2 \log \phi} \right) \quad (22)$$

We find that r_0 calculated from Eq. (22) is almost a factor of 2 larger than that measured from the SEM images. This can be attributed to the likelihood that some fraction of the fiber crossings judged by the naked eye is not indicative of true junction points. However, use of Eq. (22) implies that the determination of fiber modulus becomes dependent on mat thickness, since the experimentally measured porosity ϕ depends on this quantity as well. Confronted with these uncertainties, we have settled on the use of Eq. (22) for the determination of r_0 values, shown in Table 2, as the lesser source of error.

However, image processing or other methods to determine the average distance between true junctions directly, without recourse to measurement of porosity, is an area ripe for further development. Using the values of d , R and r_0 reported in Table 2, the stiffness ratio SR was calculated by Eq. (20) and finally the Young's moduli of fibers, E_f , based on the model for curved fibers, were determined. These are listed in Table 2 and plotted in Fig. 5 as filled circles; the agreement with the data measured for single fibers is much better.

In accord with the earlier work of Hearle and coworkers [8,9] and Engelmayer and Sacks [15], the role of fiber curvature on the properties of nonwoven fabrics can be dramatic. In contrast with that work, where fiber curvature was introduced by mechanical crimping, fiber curvature is observed here to be a function of fiber diameter, increasing with decreasing fiber diameter solely as a consequence of the low flexural rigidity of the submicron diameter fibers formed by the electrospinning process. Such curvature may be a consequence of an Euler buckling phenomenon that occurs upon compression of fibers upon impingement with the collector [24] or a feature of the whipping instability itself [16]. Either way, the quartic dependence of area moment of inertia on fiber diameter is more than sufficient to offset the factor of 2 increase in the intrinsic Young's modulus, which was previously shown to be attributable to improvements in molecular orientation in the most highly drawn electrospun fibers [4], to account for the curvature observed in fibers below 0.5 μm diameter. As a consequence, the Young's moduli of electrospun mats are found to be relatively insensitive to fiber diameter.

5. Conclusion

We conducted a systematic study of the dependence of the Young's modulus of electrospun nonwoven fabrics on the diameters of the fibers, and found that the nonwoven fabrics comprising smaller diameter fibers do not show enhanced Young's moduli compared to those comprising larger fibers. We identified four important features of the nonwoven mat that significantly affect the Young's modulus of nonwoven fabrics: the porosity (or basis weight), fiber diameter, radius of the curvature, and the distance between junctions where fibers cross. Of these, perhaps the most noteworthy is the significant effect of finite radius of curvature; the resulting deformation by bending and

unbending of fibers accounts for the significantly more compliant behavior of the mats, despite the increases in fiber modulus with decreasing fiber diameter, previously observed. The electrospinning process or post-treatment can be modified to some extent in order to change one or several of these parameters. For example, one can envision fusing or welding the fibers by thermal treatment, vapor treatment or residual solvent in order to decrease the junction length. Improvements in the microstructural modeling of nonwovens fabrics involving the bending and unbending of fibers are also underway [17]. This study provides a set of relatively simple analytical equations that can be used to determine the modulus of a mat in terms of the constituent fiber properties and curvature, or alternatively to estimate the Young's moduli of fibers from experimental measurements of the properties of the nonwoven fabrics. This is especially useful in the study of electrospun nanofibers, where equipment limitations and the difficulties of handling such small fibers individually severely complicate the direct measurement of single fiber moduli.

Acknowledgements. We wish to thank Matthew Mannarino and Dr. Jian Yu for their helpful advice regarding electrospinning. This research was supported by the U.S. Army through the Institute for Soldier Nanotechnologies (ISN), under contract ARO W911NF-07-D-0004 with the U.S. Army Research Office.

References

- [1] Shin YM, Hohman MM, Brenner MP, Rutledge GC. *Appl. Phys. Lett.* 2001;78(8):1149-1151.
- [2] Huang ZM, Zhang YZ, Kotaki M, Ramakrishna S. *Composites Science and Technology* 2003;63: 2223-2253.
- [3] Li D, Xia Y. *Adv. Mater.* 2004;16:1151-1170.
- [4] Pai CL, Boyce MC, Rutledge GC. *Polymer* 2011;52:2295.
- [5] Li L, Bellan LM, Craighead HG, Frey MW. *Polymer* 2006;47:6208-6217.
- [6] Jearanaisilawong P, Ph.D. thesis at MIT,2008;19-23.
- [7] Backer S, Petterson DR. *Textile Research Journal* 1960;30:704-711.
- [8] Hearle JWS, Stevenson PJ. *Textile Research Journal* 1964;34(3):181-191.

- [9] Hearle JWS, Newton A. Textile Research Journal 1967;37:778-797.
- [10] Lee SM, Argon AS. Journal of the Textile Institute 1983;74:1-37.
- [11] Britton PN, Sampson AJ, Elliott CF, Graben HW, Gettys WE. Textile Research Journal 1983;53:363-368.
- [12] Arslan M, Boyce MC. Journal of Applied Mechanics 2006;73:536-543.
- [13] Qi HJ, Ortiz C, Boyce MC. Journal of Engineering Materials and Technology 2006;128:509-518.
- [14] Adanur S, Liao T. Textile Research Journal 1999;69(11):816-824.
- [15] Engelmayer GC Jr, Sacks MS. Journal of Biomechanical Engineering 2006;128:610-622.
- [16] Hohman MM, Shin M, Rutledge GC, Brenner MP. Phys. Fluids 2001;13(8):2221-2236.
- [17] Silberstein MN, Pai CL, Rutledge GC, Boyce MC, J. Mech. Phys. Solids, (in press).
- [18] Palmer JS, Ph.D. thesis at MIT,2008;172-175.
- [19] Cox HL. Brit. J. Appl. Phys. 1952;3:72-79.
- [20] Bashford D. Thermoplastics: directory and databook, Springer,1997;329.
- [21] Pham QP, Sharma U, Mikos AG. Biomacromolecules 2006;7,2796-2805.
- [22] Rutledge GC, Lowery JL, Pai CL. Journal of Engineered Fibers and Fabrics 2009;4(3):1-13.
- [23] Sampson WW. J. Mater. Sci. 2003;38:1617-1622.
- [24] Han T, Reneker DH, Yarin, AL, Polymer 2007;48(20):6064-6076.

Appendix. Due to the static manner in which fiber mats were collected during electrospinning, the electrospun nonwoven fabrics are expected to be randomly oriented within the plane of the fabric. This was confirmed by image analysis of SEM images for mats of different fiber size, using the algorithm proposed by Jahne [A1]. No significant deviation from random orientation was observed in the distributions of fiber orientation for mats of small, intermediate or large fibers, which can be seen in Figure A1. The calculated $\langle \sin^2 \theta_0 \rangle$ from image analysis are 0.515 for fiber diameter (d) = 170 nm; 0.474 for $d = 1387$ nm; and 0.520 for $d = 3643$ nm, which are close to the assumed value of 0.5 for randomly distributed nonwoven fabrics in Eq. (9) of the main text.

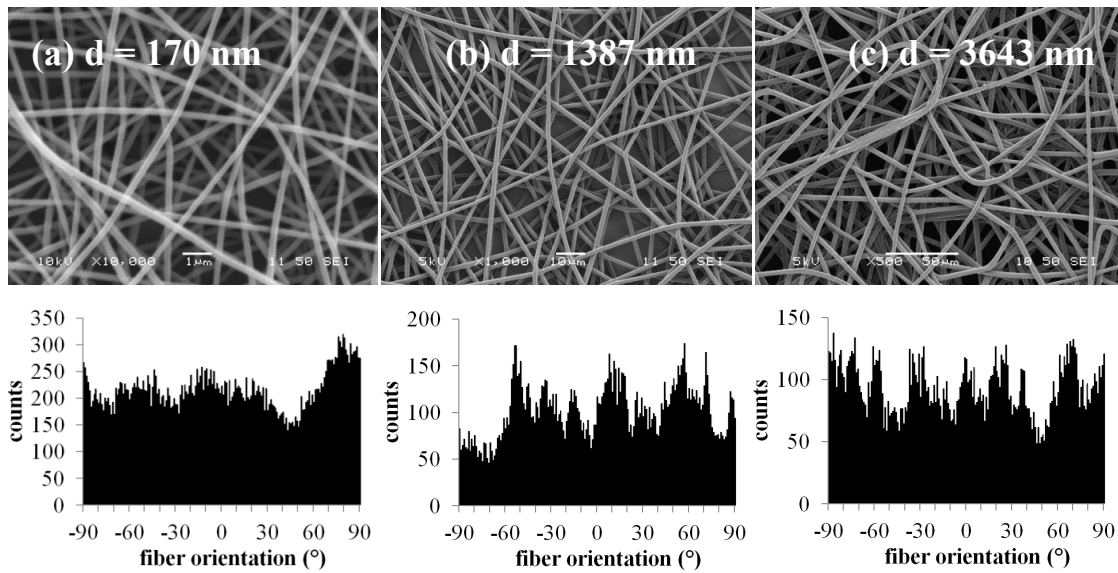


Figure A1. Distribution of fiber orientation within randomly distributed nonwoven fabrics. Counts and angles were determined by image analysis.

[A1] Jahne, B. in Digital Image Processing, Springer: New York, 2005.